ACS OMEGA

http://pubs.acs.org/journal/acsodf

Article

Hypoglycemic and Hypolipidemic Effects of Malonyl Ginsenosides from American Ginseng (*Panax quinquefolius* L.) on Type 2 Diabetic Mice

Zhi Liu,*,‖ Chun-Yuan Qu,‖ Jia-Xin Li, Yan-Fang Wang, Wei Li, Chong-Zhi Wang, Dong-Sheng Wang, Jia Song, Guang-Zhi Sun,* and Chun-Su Yuan

Cite This: *ACS Omega* 2021, 6, 33652−33664

Read Online

ACCESS | Metrics & More | Article Recommendations

ABSTRACT: American ginseng (*Panax quinquefolius* L.) is popularly consumed as traditional herbal medicine and health food for the treatment of type 2 diabetes mellitus (T2DM). Malonyl ginsenosides (MGR) are the main natural ginsenosides in American ginseng. However, whether the malonyl ginsenosides in *P. quinquefolius* (PQ-MGR) possess antidiabetic effects has not been explored yet. In this study, the antidiabetic effects and the underlying mechanism of PQ-MGR in high-fat diet/streptozotocin (HFD/STZ)-induced T2DM mice were investigated. The chemical composition was analyzed by high-performance liquid chromatography-electrospray ionization tandem mass spectrometry (HPLC-ESI-MS/MS). Our results showed that 14 malonyl ginsenosides were identified in the PQ-MGR. Among them, the content of m-Rb_1 represented about 77.4% of the total malonyl ginsenosides. After a 5-week experiment, the PQ-MGR significantly reduced the fasting blood glucose (FBG), triglyceride (TG), total cholesterol (TC), low-density lipoprotein cholesterol (LDL-C), nonesterified fatty acid (NEFA), alanine transaminase (ALT), and aspartate transaminase (AST) levels and improved glucose tolerance and insulin resistance. Furthermore, Western blot analysis demonstrated that the protein expressions of p-PI3K, p-AKT, p-AMPK, p-ACC, $PPAR_\gamma$, and GLUT4 in the liver and skeletal muscle were significantly upregulated after PQ-MGR treatment. In contrast, the protein expressions of p-IRS1 and p-JNK were significantly downregulated. Our results revealed that PQ-MGR could ameliorate glucose and lipid metabolism and insulin resistance in T2DM via regulation of the insulin receptor substrate-1/phosphoinositide3-kinase/protein-kinase B (IRS1/PI3K/Akt) and AMP-activated protein kinase/acetyl-CoA carboxylase (AMPK/ACC) pathways. These findings suggest that PQ-MGR may be used as an antidiabetic candidate drug for T2DM treatment.

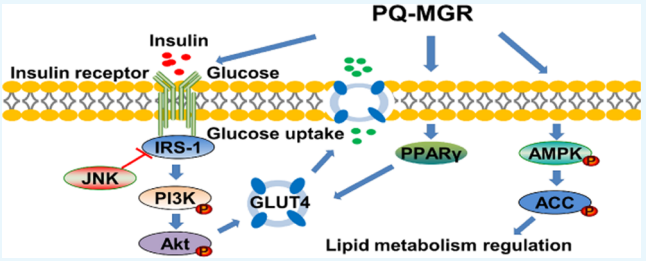

INTRODUCTION

Diabetes mellitus (DM) is a prevalent chronic metabolic disease and a global public health concern classified into insulin-dependent diabetes mellitus (type 1 diabetes mellitus, T1DM) and non-insulin-dependent diabetes mellitus (type 2 diabetes mellitus, T2DM).[1] Among them, T2DM has become a major threat to public health since 90−95% of diabetic patients are suffering from this type of disease. It is mostly characterized by deficiency of insulin secretion and/or progressive insulin resistance.[2,3] According to the International Diabetes Federation (IDF), the number of people with diabetes was 463 million worldwide in 2019 and projected to increase to 700 million by 2045.[4] As for T2DM therapy, there have been a series of antidiabetic drugs, including metformin hydrochloride, sulfonylureas, glucosidase inhibitors, thiazolidinedione, and so on.[5] However, the long-term use of these chemical synthetic drugs could lead to several unfavorable side effects, such as edema, weight gain, nausea, and potentially diarrhea.[6,7] Therefore, it is vital to find out safe, affordable, and effective natural substances with antidiabetic activities for T2DM patients.

Insulin resistance (IR) is the driving factor that leads to the development of type 2 diabetes.[8] IR is defined as the state when the body does not respond well to insulin in its insulin target tissues, such as the liver, skeletal muscle, and adipose tissue.[9] The insulin receptor substrate-1/phosphoinositide3-kinase/protein-kinase B (IRS1/PI3K/Akt) signal pathway, by which insulin maintains normal physiological function for glucose uptake and metabolism, plays an important role in insulin signaling transduction.[10] Insulin signal transduction is

Received: August 26, 2021
Accepted: November 22, 2021
Published: December 6, 2021

Table 1. Ginsenosides Identified in PQ-MGR Extract by HPLC-ESI-MS/MS[a]

no.	identification	T_R (min)	formula	M − H	MS^2 fragment ions (m/z)
1	malonyl-Rg_1	25.52	$C_{45}H_{74}O_{17}$	885.5	885[M − H]$^-$, 841[M − H − CO_2]$^-$, 799[M − H − Mal]$^-$, 781[M − H − Mal − H_2O]$^-$, 637[M − H − Mal − Glc]$^-$, 475[M − H − Mal − 2Glc]$^-$
2	malonyl-Re	25.96	$C_{51}H_{84}O_{21}$	1031.5	1031[M − H]$^-$, 987[M − H − CO_2]$^-$, 945[M − H − Mal]$^-$, 783[M − H − Mal − Glc]$^-$, 637[M − H − Mal − Glc − Rha]$^-$, 475[M − H − Mal − 2Glc − Rha]$^-$
3	Rb_1	40.14	$C_{54}H_{92}O_{23}$	1107.9	1107[M − H]$^-$, 945[M − H − Glc]$^-$, 783[M − H − 2Glc]$^-$, 621[M − H − 3Glc]$^-$, 459[M − H − 4Glc]$^-$
4	malonyl-Rb_1	40.96	$C_{57}H_{94}O_{26}$	1193.8	1193[M − H]$^-$,1149[M − H − CO_2]$^-$, 1107[M − H − Mal]$^-$, 945[M − H − Mal − Glc]$^-$, 783[M − H − Mal − 2Glc]$^-$, 621[M − H − Mal − 3Glc]$^-$, 459[M − H − Mal − 4Glc]$^-$
5	Ro	42.05	$C_{49}H_{80}O_{18}$	955.8	955[M − H]$^-$, 793[M − H − Glc]$^-$
6	malonyl-Rc	42.44	$C_{56}H_{92}O_{25}$	1163.6	1163[M − H]$^-$, 1119[M − H − CO_2]$^-$, 1077[M − H − Mal]$^-$, 945[M − H − Mal − Ara(f)]$^-$, 783[M − H − Mal − Ara(f) − Glc]$^-$, 621[M − H − Mal − Ara(f) − 2Glc]$^-$, 459[M − H − Mal − Ara(f) − 3Glc]$^-$
7	malonyl-Rb_1 isomer	43.26	$C_{57}H_{94}O_{26}$	1193.9	1193[M − H]$^-$, 1149[M − H − CO_2]$^-$, 1107[M − H − Mal]$^-$, 945[M − H − Mal − Glc]$^-$, 783[M − H − Mal − 2Glc]$^-$, 621[M − H − Mal − 3Glc]$^-$, 459[M − H − Mal − 4Glc]$^-$
8	malonyl-Rb_2	44.19	$C_{56}H_{92}O_{25}$	1163.5	1163[M − H]$^-$, 1119[M − H − CO_2]$^-$, 1077[M − H − Mal]$^-$, 945[M − H − Mal − Ara(p)]$^-$, 783[M − H − Mal − Ara(p) − Glc]$^-$, 621[M − H − Mal − Ara(p) − 2Glc]$^-$, 459[M − H − Mal − Ara(p) − 3Glc]$^-$
9	malonyl-Rb_3	44.90	$C_{56}H_{92}O_{25}$	1163.5	1163[M − H]$^-$,1119[M − H − CO_2]$^-$, 1077[M − H − Mal]$^-$, 945[M − H − Mal − Xyl]$^-$, 783[M − H − Mal − Xyl − Glc]$^-$, 621[M − H − Mal − Xyl − 2Glc]$^-$, 459[M − H − Mal − Xyl − 3Glc]$^-$
10	malonyl-Rc isomer	45.11	$C_{56}H_{92}O_{25}$	1163.5	1163[M − H]$^-$, 1119[M − H − CO_2]$^-$, 1077[M − H − Mal]$^-$, 945[M − H − Mal − Ara(f)]$^-$, 783[M − H − Mal − Ara(f) − Glc]$^-$, 621[M − H − Mal − Ara(f) − 2Glc]$^-$, 459[M − H − Mal − Ara(f) − 3Glc]$^-$
11	malonyl-Rb_2 isomer	45.29	$C_{56}H_{92}O_{25}$	1163.5	1163[M − H]$^-$, 1119[M − H − CO_2]$^-$, 1077[M − H − Mal]$^-$, 945[M − H − Mal − Ara(p)]$^-$, 783[M − H − Mal − Ara(p) − Glc]$^-$, 621[M − H − Mal − Ara(p) − 2Glc]$^-$, 459[M − H − Mal − Ara(p) − 3Glc]$^-$
12	malonyl-Rb_3 isomer	46.16	$C_{56}H_{92}O_{25}$	1163.5	1163[M − H]$^-$, 1119[M − H − CO_2]$^-$, 1077[M − H − Mal]$^-$, 945[M − H − Mal − Xyl]$^-$, 783[M − H − Mal − Xyl − Glc]$^-$, 621[M − H − Mal − Xyl − 2Glc]$^-$, 459 [M − H − Mal − Xyl − 3Glc]$^-$
13	malonyl-Rd	46.77	$C_{51}H_{84}O_{21}$	1031.7	1031[M − H]$^-$, 987[M − H − CO_2]$^-$, 945[M − H − Mal]$^-$, 783[M − H − Mal − Glc]$^-$, 621[M − H − Mal − 2Glc]$^-$, 459[M − H − Mal − 3Glc]$^-$
14	malonyl-Rd isomer	47.92	$C_{51}H_{84}O_{21}$	1031.7	1031[M − H]$^-$, 987[M − H − CO_2]$^-$, 945[M − H −Mal]$^-$, 783[M − H − Mal − Glc]$^-$, 621[M − H − Mal − 2Glc]$^-$, 459[M − H − Mal − 3Glc]$^-$
15	malonyl-Rd isomer	49.88	$C_{51}H_{84}O_{21}$	1031.7	1031[M − H]$^-$, 987[M − H − CO_2]$^-$, 945[M − H − Mal]$^-$, 783[M − H − Mal − Glc]$^-$, 621[M − H − Mal − 2Glc]$^-$, 459[M − H − Mal − 3Glc]$^-$
16	malonyl-Rd isomer	50.43	$C_{51}H_{84}O_{21}$	1031.7	1031[M − H]$^-$, 987[M − H − CO_2]$^-$, 945[M − H − Mal]$^-$, 783[M − H − Mal − Glc]$^-$, 621[M − H − Mal − 2Glc]$^-$, 459[M − H − Mal − 3Glc]$^-$

[a]Ara(p), α-L-arabinose (pyranose); Ara(f), α-L-arabinose (furanose); Glc, β-D-glucose; Mal, malonyl; Rha, α-L-rhamnose; Xyl, β-D-xylose.

initiated when insulin binds to the insulin receptor such that the phosphorylated insulin receptor can stimulate the tyrosine phosphorylation of IRS1 to transmit insulin signals, which then phosphorylate its downstream protein PI3K and Akt.[11] Moreover, C-Jun N-terminal kinases (JNKs) play an essential role as the mediator of insulin resistance.[12] Previous studies have reported that JNKs mediate serine phosphorylation of IRS1, while Ser307 phosphorylation of IRS1 leads to defective IRS1 tyrosine phosphorylation and decreased phosphatidylinositol 3-kinase (PI3K)/protein kinase B (Akt) signaling in response to insulin receptor activation, thereby causing insulin resistance.[13,14]

AMP-activated protein kinase (AMPK) is one of the crucial targets for metabolic disorders that have been associated with the regulation of lipid metabolism and systemic glucose homeostasis.[15] AMPK is a heterotrimer consisting of an α catalytic subunit and two regulatory β and γ subunits, and the activation of AMPK depends on α subunit phosphorylation.[16] Acetyl-CoA carboxylase (ACC) is the rate-limiting enzyme participating in the synthesis of fatty acids and acts as the essential downstream effector of the AMPK signaling pathway.[17] The activation of AMPK could stimulate the increase of ACC phosphorylation.[18] Thus, regulating the IRS-1/PI3K/Akt and AMPK/ACC signal pathways could be considered as an effective therapeutic strategy to treat T2DM.

American ginseng (*Panax quinquefolius* L.) is a perennial herb of the Araliaceae family, cultivated in the United States and China as well as in Canada and France.[19] Pharmacological investigations have shown that American ginseng possesses a large variety of pharmacological properties, such as antidiabetes, antioxidant, anti-inflammatory, and antitumor effects.[20−23] It has been widely used for herbal medicine and health foods. As one of the best-selling herbs in the world, the root of American ginseng is well documented in internationally recognized pharmacopeia such as the China Pharmacopeia, the US Pharmacopeia, and the European Pharmacopoeia. The major bioactive ingredients of American ginseng are ginsenosides, a group of steroidal saponins, which includes neutral ginsenosides (e.g., Rb_1, Rb_2, Rc, Rd, Rg_3, Rh_2, and C-K) and malonyl ginsenosides (e.g., m-Rb_1, m-Rb_2, m-Rc, m-Rd, m-Rg_1, and m-Re).[24] To date, more than 150 ginsenosides have been identified from several plants of the genus Panax.[25]

More recently, a series of experimental studies indicated that neutral ginsenosides from American ginseng possessed significant antidiabetic effects.[23] They are believed to be the major chemical components responsible for antidiabetic activities of American ginseng. For example, ginsenoside Rb_1 has been reported to reduce fasting blood glucose (FBG) levels and triglyceride accumulation and ameliorate insulin and leptin sensitivities.[26,27] Ginsenoside Rb_2 could obviously improve glucose metabolism and inhibit gluconeogenesis and hepatic lipid accumulation.[28,29] Ginsenoside Re could also decrease FBG levels, food intake, and fasting serum insulin levels and improve glucose tolerance and insulin resistance.[30,31] However,

https://doi.org/10.1021/acsomega.1c04656
ACS Omega 2021, 6, 33652−33664

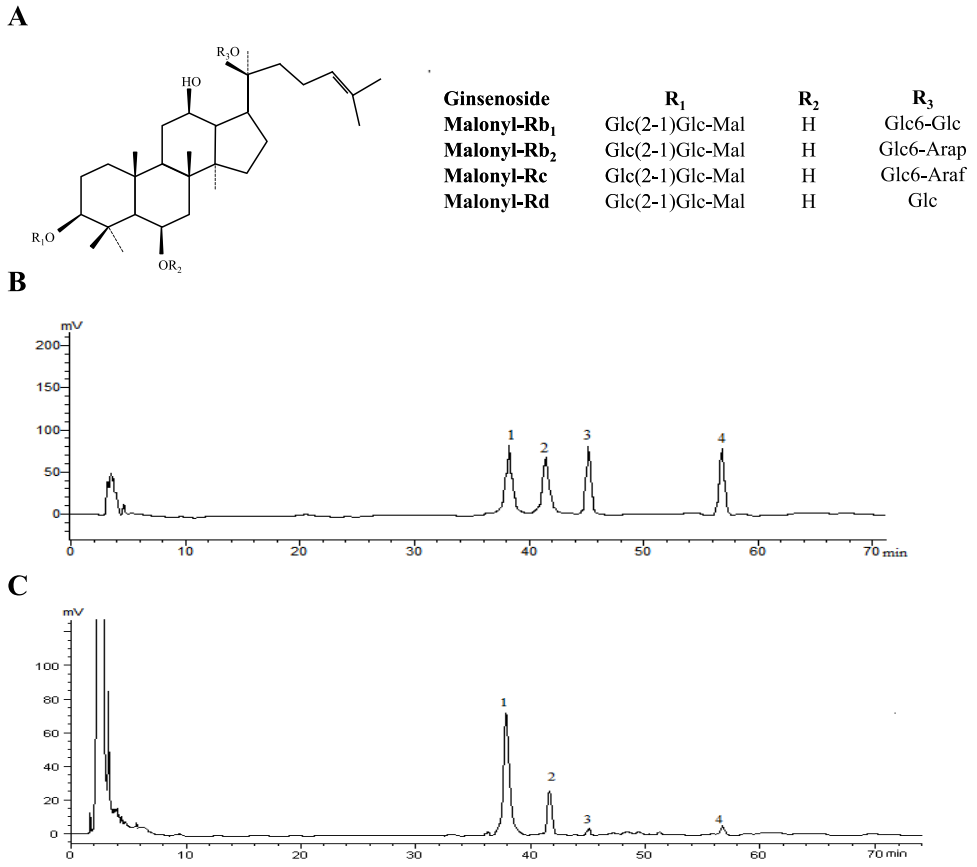

Figure 1. Chemical structures of the malonyl ginsenosides in American ginseng (A); HPLC chromatograms of mixed malonyl ginsenoside standards (B) and PQ-MGR extract purified by macroreticular resin D-101 and cation exchange resin SP20ss (C). Peaks: 1−4, malonyl-Rb_1, malonyl-Rc, malonyl-Rb_2, and malonyl-Rd, respectively.

the pharmacological and clinical researches on the antidiabetic effect of ginsenosides in American ginseng are primarily focused on neutral ginsenosides. Whether the malonyl ginsenosides in *P. quinquefolius* (PQ-MGR) possess antidiabetic effects has not been explored yet.

Malonyl ginsenosides (MGR) are natural ginsenosides that exist in both fresh and air-dried American ginseng. Previous published studies have shown that the content of PQ-MGR accounted for more than 50% of the total saponins.[32] However, malonyl ginsenosides are not easily separated, identified, or detected, unlike the neutral ginsenosides. Therefore, the chemical and pharmacological studies of malonyl ginsenosides are lacking. The true ginsenosides of American ginseng and pharmacological studies of ginsenosides were underestimated by ignoring PQ-MGR. Moreover, the different species of ginseng contain distinct malonyl ginsenoside profiles. Previous studies have reported that malonyl ginsenosides were effective chemical markers to differentiate Panax species. *P. quinquefolius* had a level of m-Rb_2, m-Rb_3, and m-Rc relative to m-Rb_1 lower than *Panax ginseng*.[33] Therefore, malonyl ginsenosides from different species may exhibit different biological and pharmacological activities. Our previous study revealed that malonyl ginsenosides from the *P. ginseng* root (PG-MGR) possessed a strong hypoglycemic effect on the streptozotocin-induced type 2 diabetic rat. However, the underlying mechanism is not yet clear. In the present study, we reported the hypoglycemic and hypolipidemic effects of PQ-MGR and explored the underlying mechanism in diabetic conditions induced by high-fat diet/streptozotocin (HFD/STZ) in mice for the first time.

RESULTS

Identification of Ginsenosides in the PQ-MGR Extract by High-Performance Liquid Chromatography-Electrospray Ionization Tandem Mass Spectrometry (HPLC-ESI-MS/MS). Under the optimal chromatographic and MS conditions, the malonyl ginsenosides in the PQ-MGR extract were analyzed by HPLC-ESI-MS. A total of 14 major malonyl ginsenosides were identified, five of which (m-Rb_1, m-Rb_2, m-Rb_3, m-Rc, and m-Rd) were confirmed by comparison of retention times as well as MS data of these reference compounds, whereas the others were tentatively assigned by matching the retention behavior and characteristic fragment ions with those of the published known malonyl ginsenosides in American ginseng. The details of identified malonyl ginsenosides are summarized in Table 1. Compound 4 (RT 40.96 min) was used as an example to illustrate the structural characterization of ginsenosides. In MS full scan under negative-ion mode, compound 4 displayed a deprotonated ion $[M - H]^-$ (m/z 1193) and a product ion $[M - CO_2 - H]^-$ (m/z 1149) with high abundance. When suffering from a higher collision energy, a neutral loss of 86 Da ($C_3H_2O_3$) was observed to produce product ion $[M - H - C_3H_2O_3]^-$ (m/z 1107). The neutral eliminations of CO_2 and $C_3H_2O_3$ were found typical for the characterization of malonyl ginsenosides. Moreover, the rest of the characteristic fragment ions at m/z 945, 783, 621, and 459 were assigned due to the eliminations

https://doi.org/10.1021/acsomega.1c04656
ACS Omega 2021, 6, 33652−33664

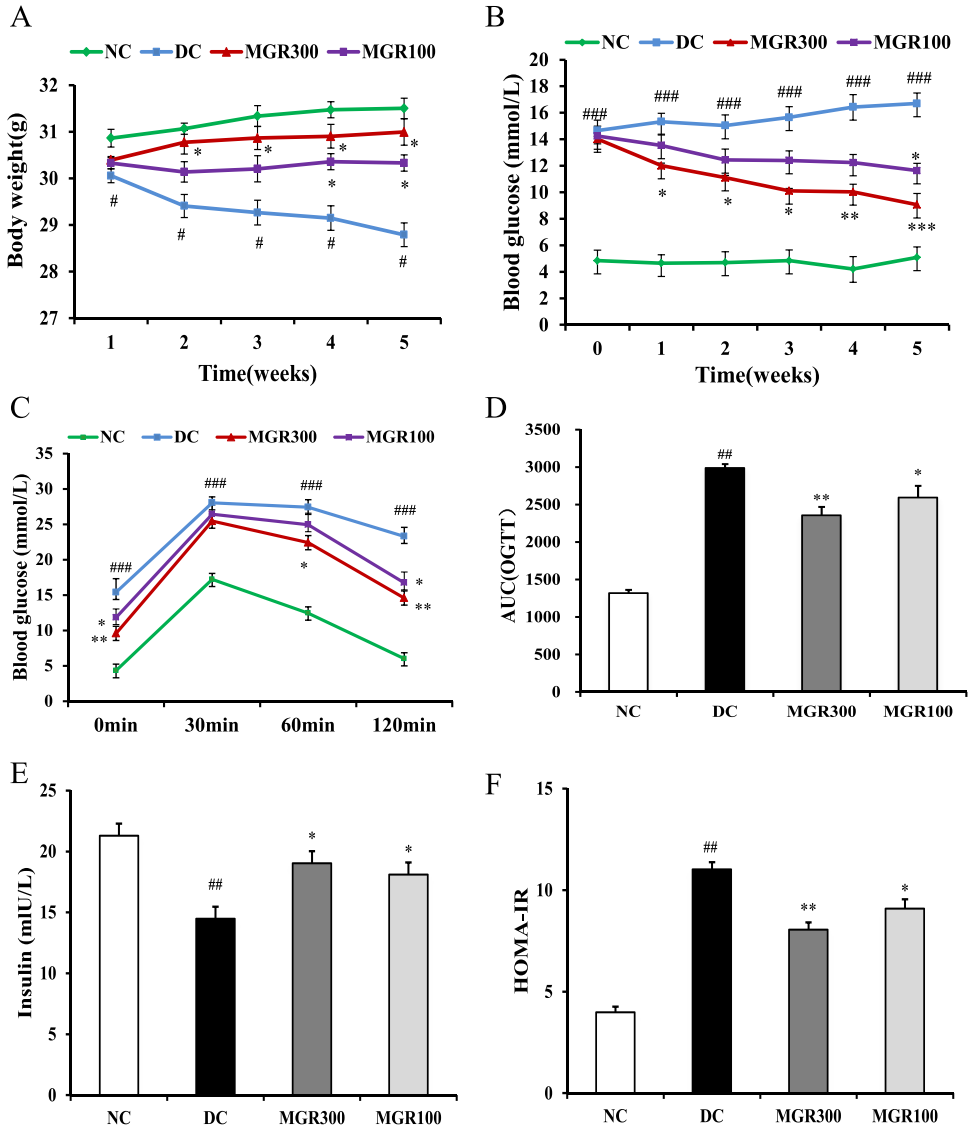

Figure 2. Effects of PQ-MGR on body weight (A); fasting blood glucose levels (B); oral glucose tolerance (OGTT) (C); area under curve (AUC) (D); serum insulin content (E); and homeostatic model assessment-insulin resistance (HOMA-IR) (F) in HFD- and STZ-induced diabetic mice. Data are described as mean ± standard deviation (SD) (n = 10). $^{###}p < 0.001$, $^{##}p < 0.01$, $^{#}p < 0.05$ compared with normal control group. $^{***}p < 0.001$, $^{**}p < 0.01$, $^{*}p < 0.05$ compared with diabetic control group.

of Glc, 2 × Glc, 3 × Glc, and 4 × Glc, respectively. Therefore, the structure of compound 4 was unambiguously identified as malonyl ginsenoside Rb_1 by comparison of retention times as well as MS data of its authentic standard. In the same way, the chemical structures of the other ginsenosides were identified as depicted in Table 1.

HPLC Analysis of PQ-MGR Extract. As shown in Figure 1, the contents of malonyl ginsenosides from PQ-MGR extract were examined by high-performance liquid chromatography (HPLC). The results showed that PQ-MGR extract was 82.77% pure with 63.4% recovery. There were 64.08 ± 0.35 mg/100 mg of m-Rb_1, 15.89 ± 0.13 mg/100 mg of m-Rc, 1.02 ± 0.09 mg/100 mg of m-Rb_2, and 1.78 ± 0.15 mg/100 mg of m-Rd in the final extract. Among them, the content of m-Rb_1 represented about 77.4% of the total malonyl ginsenosides. Therefore, m-Rb_1 was the most abundant malonyl ginsenoside in PQ-MGR extract. However, the contents of neutral ginsenosides were relatively low, and they were not detected by HPLC at all.

Effects of PQ-MGR on Body Weight, FBG, OGTT, and Serum Insulin Levels. As shown in Figure 2A, the body weight in diabetic control group mice significantly decreased than that in the normal control group ($p < 0.05$). Compared with the diabetic control group, the body weights of mice in the PQ-MGR treatment groups were increased. According to monitoring changes in body weight and daily behavior during treatment, no toxicity was observed in any treatment group.

The effect of PQ-MGR on glucose metabolism was evaluated by FBG levels, which were measured every week after 12 h of food removal. As shown in Figure 2B, diabetic mice presented significant hyperglycemia compared with the normal control mice at week 0 ($p < 0.001$). After treatment with PQ-MGR at 300 and 100 mg/kg, the FBG levels in the 300 mg/kg PQ-MGR-treated group were significantly lower than the diabetic control group from weeks 1 to 4, and at week 5, the levels were further reduced by 45.74% ($p < 0.001$). In the group treated with PQ-MGR 100 mg/kg, the FBG levels decreased significantly ($p < 0.05$) only at week 5. The

https://doi.org/10.1021/acsomega.1c04656
ACS Omega 2021, 6, 33652−33664

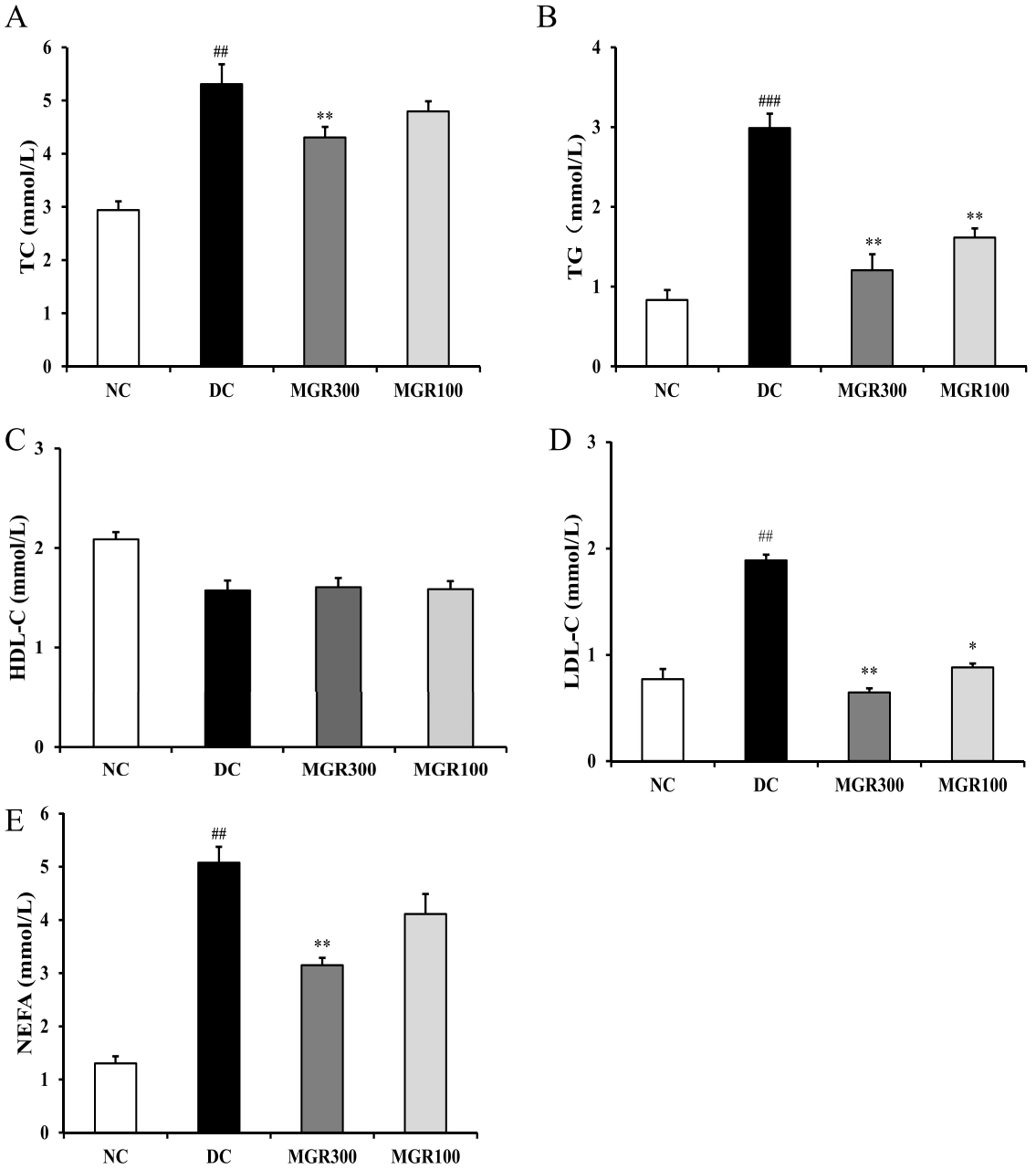

Figure 3. Effects of PQ-MGR on serum lipids in HFD- and STZ-induced diabetic mice. TC (A); TG (B); HDL-C (C); LDL-C (D); NEFA (E). Data are described as mean ± SD (n = 10). $^{\#\#}p < 0.01$, $^{\#}p < 0.05$ compared with normal control group; $^{**}p < 0.01$, $^{*}p < 0.05$ compared with diabetic control group.

experimental results showed that PQ-MGR has a hypoglycemic effect on T2DM mice.

The results of the oral glucose tolerance test (OGTT) and the areas under the curve of OGTT (OGTT-AUC) are shown in Figure 2C,D. The initial blood glucose levels in the HFD/STZ-induced diabetic control group were significantly higher than those in the normal control group and the PQ-MGR-treated groups ($p < 0.001$). At 30 min following glucose administration, blood glucose levels spiked in all mice. Compared to 30 min, the 100 and 300 mg/kg PQ-MGR-treated mice showed 36.74% ($p < 0.05$) and 42.76% ($p < 0.01$) reduction in blood glucose levels after 120 min post-administration. Furthermore, we calculated the area under the concentration curve (AUC). PQ-MGR treatment showed significant lower values of AUC than that of the diabetic control group. The results from the present study indicated that the treatment with PQ-MGR improved glucose tolerance and blood glucose homeostasis in the HFD/STZ-induced T2DM mice.

Data for changes in serum insulin levels and HOMA-IR indexes are observed in Figure 2E,F. The diabetic control group showed a significant decrease ($p < 0.01$) in insulin levels and an increase ($p < 0.01$) in HOMA-IR indexes compared with the normal control group. After 5 weeks of treatment, the PQ-MGR-treated group showed significant improvement in the fasting insulin levels at all selected doses ($p < 0.05$). The PQ-MGR-treated group also showed significant reduction in HOMA-IR indexes. These results indicated that the administration of PQ-MGR could ameliorate insulin resistance.

https://doi.org/10.1021/acsomega.1c04656
ACS Omega 2021, 6, 33652−33664

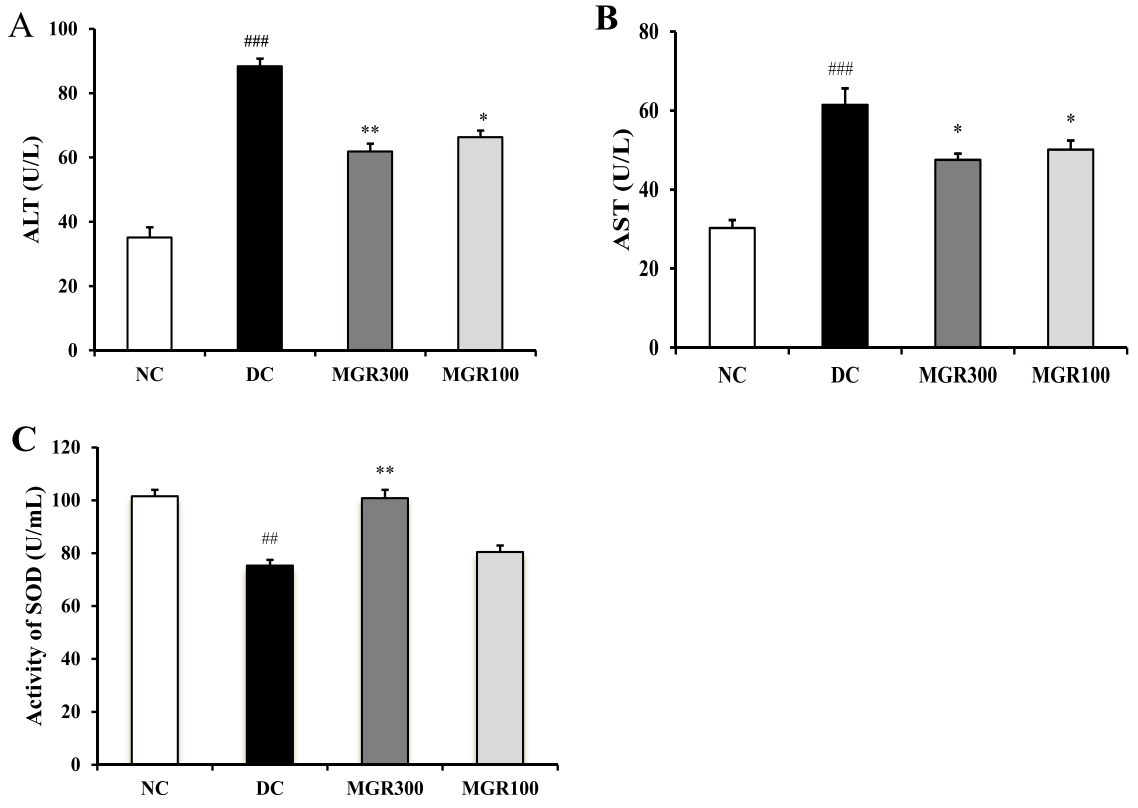

Figure 4. Effects of PQ-MGR treatment on serum ALT (A), AST (B), and superoxide dismutase (SOD) level (C) in HFD- and STZ-induced diabetic mice. Data are described as mean ± SD (n = 10). $^{###}p < 0.001$, $^{##}p < 0.01$ compared with normal control group; $^{**}p < 0.01$, $^{*}p < 0.05$ compared with diabetic control group.

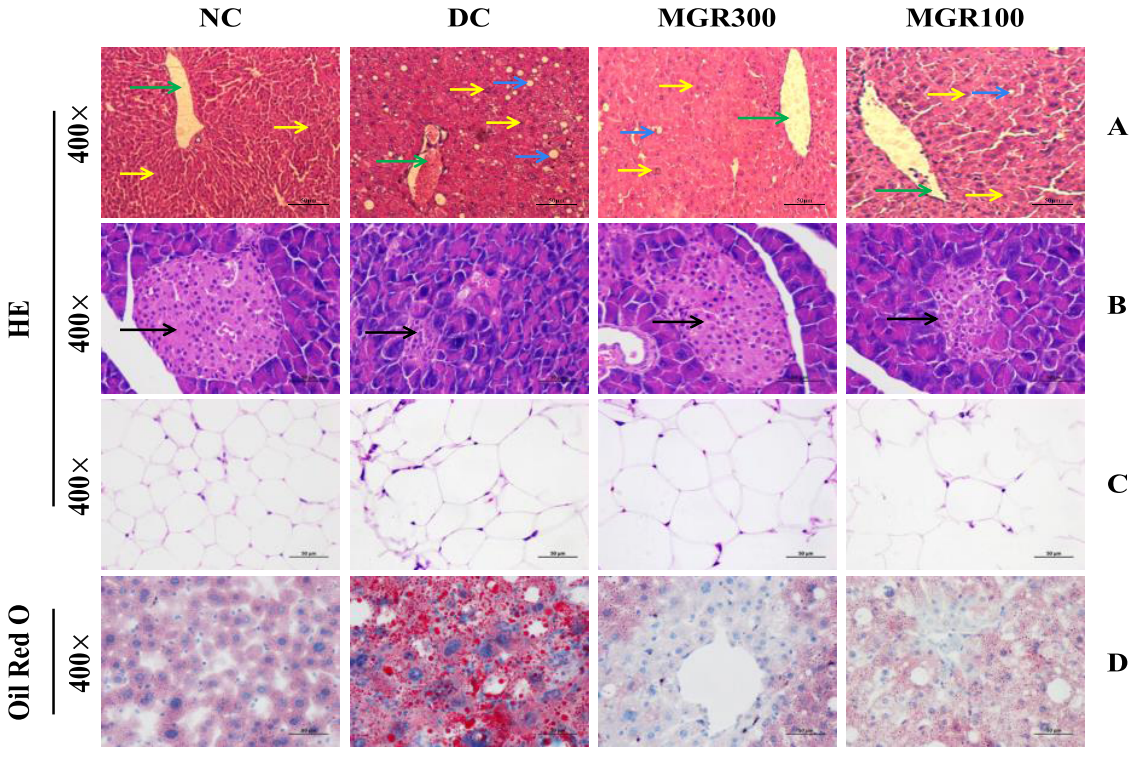

Figure 5. Effects of PQ-MGR on liver, pancreas, and adipose tissue histopathological changes in T2DM mice. H&E staining of liver (A). Green arrows indicate central veins. Yellow arrows indicate hepatocytes. Blue arrows indicate lipid droplets. H&E staining of pancreas (B). Black arrows indicate islet cells. H&E staining of adipose tissue (C). Oil red O staining of liver (D) (original magnification, 400×).

https://doi.org/10.1021/acsomega.1c04656
ACS Omega 2021, 6, 33652−33664

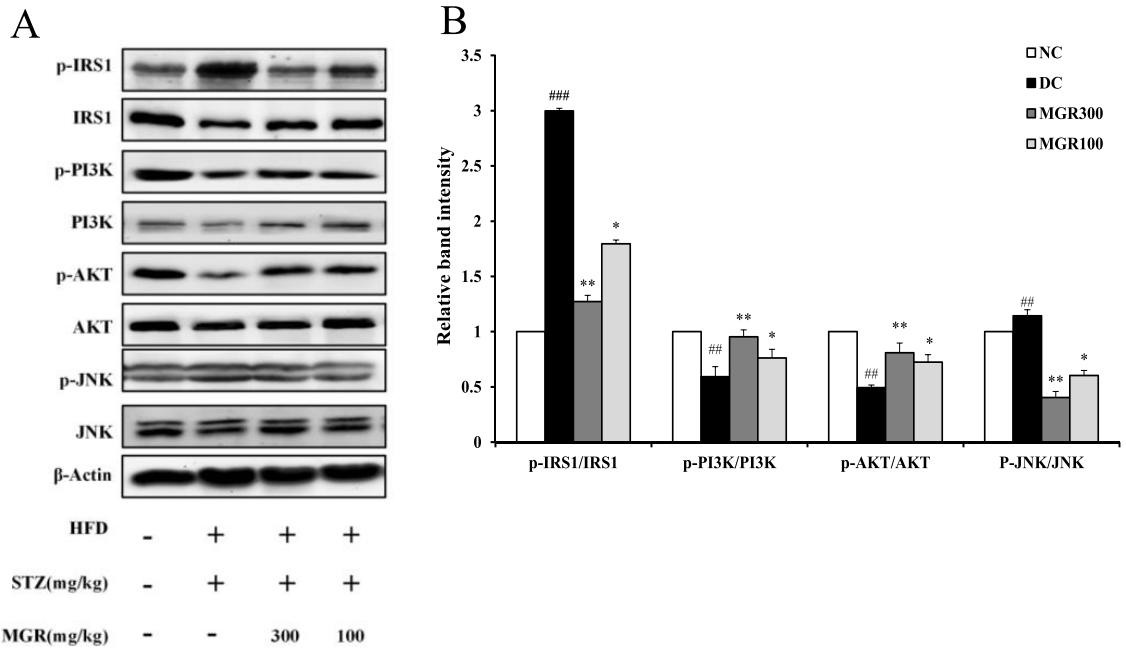

Figure 6. Effects of PQ-MGR on the IRS1/PI3K/Akt and JNK pathway in liver tissues of HFD- and STZ-induced diabetic mice. Bands of western blot (A); densitometric analysis of the p-IRS1/IRS1, p-PI3K/PI3K, p-Akt/Akt, and p-JNK/JNK ratios (B). Data are presented as mean ± SD. $^{###}p < 0.001$, $^{##}p < 0.01$ in contrast to the normal control group; $^{**}p < 0.01$, $^{*}p < 0.05$ in contrast to the diabetic control group.

Effects of PQ-MGR on Blood Lipid Levels. As shown in Figure 3, the serum levels of total cholesterol (TC), triglyceride (TG), LDL-C, and nonesterified fatty acid (NEFA) in mice from the diabetic model group increased significantly compared with that of mice from the normal control group. The TG, TC, LDL-C, and NEFA levels were significantly lower in the PQ-MGR-treated groups, particularly in the high-dose PQ-MGR-treated group, than in the diabetic control group. But, there were no changes in HDL-C levels between the PQ-MGR treatment group and the diabetic control group. Therefore, these results suggested that PQ-MGR might regulate lipid metabolism in T2DM mice.

Effects of PQ-MGR on Liver Injury. As seen in Figure 4A,B, HFD/STZ-induced diabetic mice produced severe liver injury, characterized by significant increases in serum aspartate transaminase (AST) and alanine transaminase (ALT) levels. After 5 weeks of continuous treatment, PQ-MGR-treated groups exhibited significant decreases in ALT and AST levels compared to the diabetic control group. These results showed that PQ-MGR administration effectively repaired liver injury in T2DM mice.

SOD is a crucial antioxidant that scavenges free radicals. As depicted in Figure 4C, compared to the normal control group, the serum SOD activity significantly decreased ($p < 0.01$) in diabetic control mice, indicating serious liver injury caused by lipid peroxidation. With PQ-MGR (300 mg/kg) treatment, the serum SOD activity significantly increased ($p < 0.05$) compared with that of the diabetic control group. However, PQ-MGR (100 mg/kg) treatment improved SOD activity with no significant difference.

Effects of PQ-MGR on the Histopathology in T2DM Mice. The hematoxylin and eosin (H&E) staining in the liver is shown in Figure 5A. The livers of normal control mice showed an orderly hepatic lobular architecture and substantial hepatocytes with clear nuclei, while the livers of diabetic control mice had hepatic steatosis and macrovesicular cells. After oral administration of PQ-MGR, these severe liver injuries showed a marked improvement. As shown in Figure 5B, the islets of the normal control group were round or oval cell clusters with clear boundaries. In contrast, the islet cells of the diabetic control group were damaged and shrunken with atypical cellular changes, such as irregular profile, vacuole, and inflammatory infiltration. After 5 weeks of treatment, the administration of PQ-MGR at high doses in HFD/STZ-induced diabetic mice prevented atrophy, structural damage, and the loss of islets. HE staining of adipose tissue is shown in Figure 5C. The size of adipose tissue in the T2DM mice drastically increased, and the structure was not clear compared to the normal control group. In contrast, the cell volume and structure of the PQ-MGR-treated groups were markedly alleviated. Moreover, Oil red O staining revealed that PQ-MGR significantly reduced size and accumulation of lipid droplets in the liver (Figure 5D).

Effects of PQ-MGR on IRS1/PI3K/AKT and C-Jun N-Terminal Kinases (JNK) Signaling Pathways. To further explore mechanisms of PQ-MGR on antidiabetic effects, the protein expression levels of IRS1/PI3K/AKT and JNK signaling pathways in the liver were evaluated using western blotting. As shown in Figure 6, the expressions of phosphorylation of PI3K Thr458 and AKT ser473 proteins in the PQ-MGR-treated group significantly increased compared with those in the diabetic control group, while p-IRS1 Ser307 and p-JNK Thr183/185 significantly decreased. The above results of western blot analysis revealed that PQ-MGR ameliorated insulin resistance by inhibition of JNK activity and activation of the IRS1/PI3K/AKT signaling pathway.

Effects of PQ-MGR on AMPK/ACC Pathway in the Liver and Skeletal Muscle. AMPK is a key regulator of preadipocyte differentiation and adipogenesis. To investigate whether the regulation of the AMPK/ACC pathway was involved in the hypolipemia effects of PQ-MGR, the protein expression levels of the AMPK/ACC signaling pathway in the

https://doi.org/10.1021/acsomega.1c04656
ACS Omega 2021, 6, 33652−33664

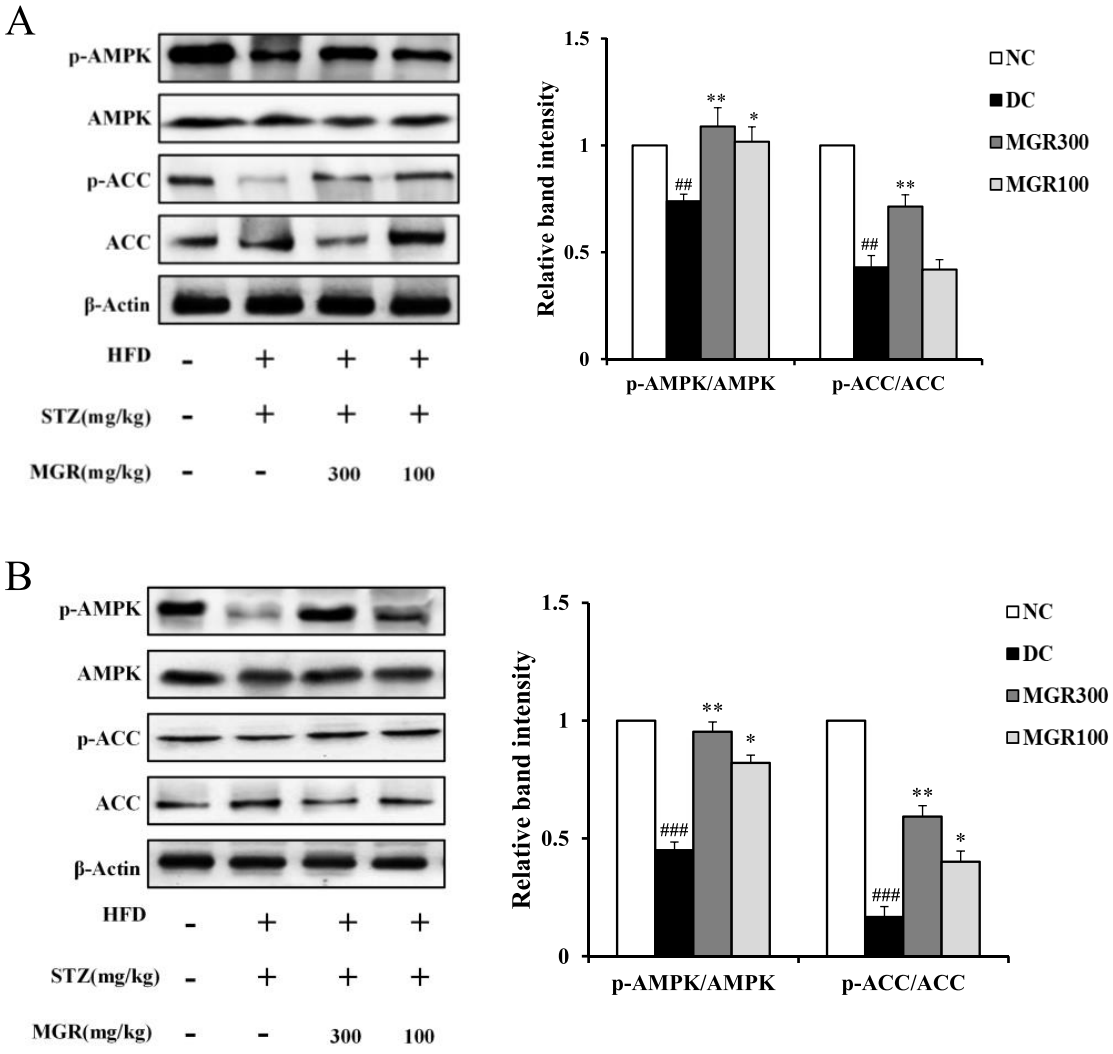

Figure 7. Effects of PQ-MGR on the AMPK/ACC pathway in the liver and skeletal muscle. Western blot analyses of AMPK/ACC in the liver with quantification (A). Western blot analyses of AMPK/ACC in skeletal muscle with quantification (B). Data are described as mean ± SD. $^{###}p < 0.001$, $^{##}p < 0.01$ in contrast to the normal control group; $^{**}p < 0.01$,$^{*}p < 0.05$ in contrast to the diabetic control group.

liver and skeletal muscle were examined by western blot analyses. As a result, the level of phosphorylated AMPK in the diabetic control mice significantly decreased, while it was remarkably enhanced in the PQ-MGR-treated group. Moreover, PQ-MGR increased the level of phosphorylated ACC, a downstream substrate of AMPK in the diabetic control group (Figure 7).

Effect of PQ-MGR on GLUT4 and PPAR$_\gamma$ in the Skeletal Muscle and Liver. The expression levels of GLUT4 and PPAR$_\gamma$ protein in the skeletal muscle and liver were detected by western blotting, as shown in Figure 8. Compared with the normal control group, the expression levels of GLUT4 and PPAR$_\gamma$ in the diabetic control group were dramatically decreased. However, following treatment with PQ-MGR, GLUT4, and PPAR$_\gamma$ protein expression in the skeletal muscle and liver of the diabetic-treated group significantly increased.

DISCUSSION

T2DM is a complex endocrine and metabolic disorder characterized by chronic hyperglycemia and impaired insulin action.[34] Although there have been a number of antidiabetic synthetic drugs for the treatment of T2DM, long-term use of these chemical synthetic drugs may cause some adverse effects. Therefore, it is of great significance to develop new natural antidiabetic agents. American ginseng is traditionally used to prevent or alleviate several human diseases. Recent studies have demonstrated that American ginseng contains various saponins, which include neutral ginsenosides and malonyl ginsenosides. Some neutral ginsenosides, such as Rb$_1$,[27] Re,[31] Rb$_2$,[28] and compound K,[35] have been shown to process antidiabetic activities. Compared to neutral ginsenosides, malonyl ginsenosides show difficulty in separation, identification, and detection. Therefore, pharmacological effects and chemical constituent studies of PQ-MGR are lacking. In this study, we successfully established an HFD/STZ-induced C57BL/6J mouse model with hyperglycemia, hyperlipidemia, and insulin resistance. Our current results showed that PQ-MGR decreased FBG levels, increased serum insulin levels, and improved insulin resistance in T2DM. To the best of our knowledge, this is the first report demonstrating that PQ-MGR could be used to treat type 2 diabetes.

https://doi.org/10.1021/acsomega.1c04656
ACS Omega 2021, 6, 33652−33664

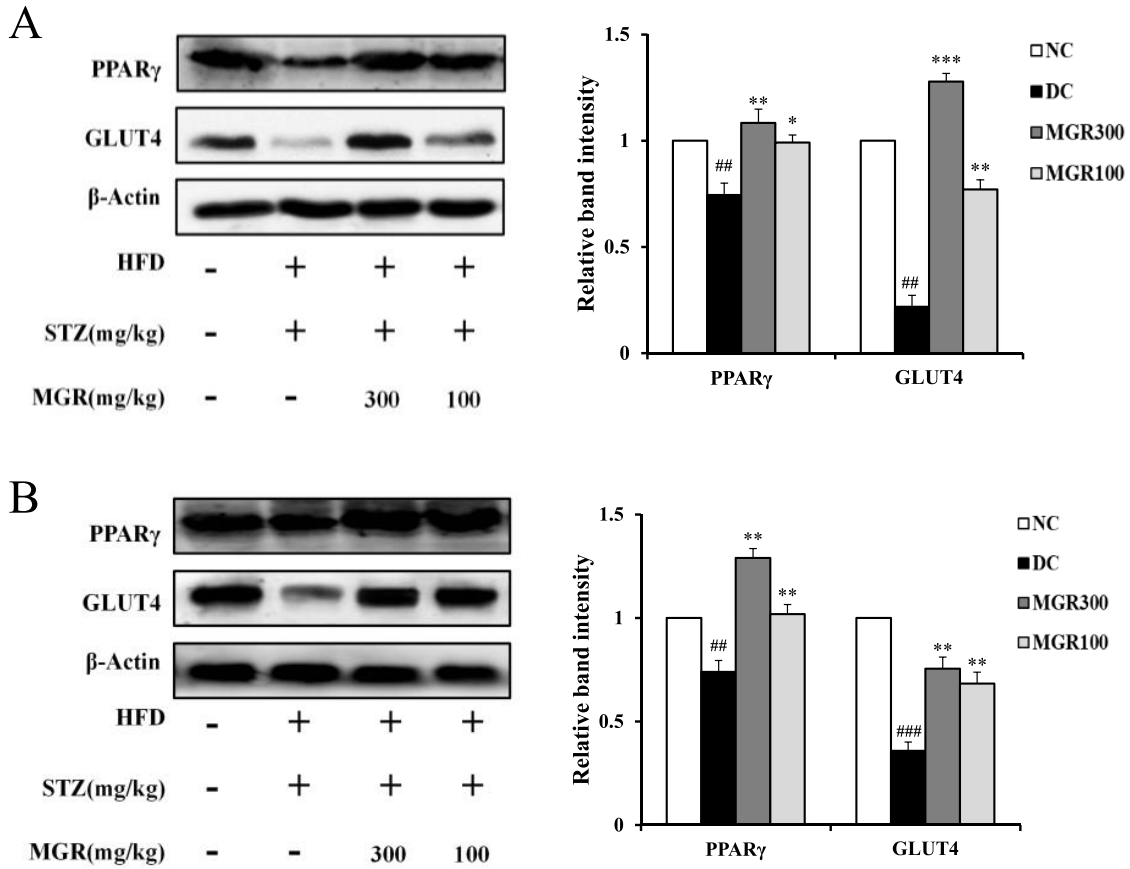

Figure 8. Effects of PQ-MGR on PPAR$_\gamma$ and GLUT4 protein levels in the liver and skeletal muscle of HFD- and STZ-induced diabetic mice. Western blot analyses of PPAR$_\gamma$ and GLUT4 in the liver with quantification (A). Western blot analyses of PPAR$_\gamma$ and GLUT4 in skeletal muscle with quantification (B). Data are described as mean ± SD. $^{###}p < 0.001$, $^{##}p < 0.01$ in contrast to the normal control group; $^{***}p < 0.001$, $^{**}p < 0.01$, $^{*}p < 0.05$ in contrast to the diabetic control group.

Insulin resistance plays a pivotal role in the development of dyslipidemia in type 2 diabetic patients because long-term insulin resistance in the adipocytes results in elevated production of free fatty acids and further causes improved formation of triglyceride.[36] Hyperinsulinemia also causes reduction in HDL-C levels and increases LDL-C levels.[37] In our study, T2DM showed significant increases in TG, TC, NEFA, and LDL-C levels and decreased levels of HDL-C, while PQ-MGR-treated groups obviously decreased TC, TG, LDL-C, and NEFA levels in diabetic mice by ameliorating insulin resistance. The results demonstrated that the administration of PQ-MGR has beneficial effects on diabetic hyperlipidemia.

The liver is a key organ in the metabolism of protein, fat, and carbohydrates and also plays an important role in insulin action and catabolism. Diabetes produces hepatic damage, which is related to increased plasmatic levels of AST and ALT.[38] Therefore, their measurements are commonly used as biomarkers for liver injury.[39] In our present study, the results revealed that treatment with PQ-MGR significantly decreased the serum levels of AST and ALT and increased the level of SOD in diabetic mice. It suggested that PQ-MGR could ameliorate pathological damage of the liver and oxidative stress.

Several signaling pathways have been identified as involved in the process of glucose metabolism. The IRS1/PI3K/AKT signaling pathway is one of the vital pathways in regulating insulin signaling and glucose metabolism.[40] IRS-1 is phosphorylated by insulin receptors to transmit insulin signals, which then activates PI3K and Akt/PKB in succession. These steps ultimately lead to GLUT4 translocation to the cell surface, reinforcing glucose transport.[41] C-Jun N-terminal kinases (JNK) play an important role in insulin target organs during the development of insulin resistance.[12] Activation of the JNK can result in insulin resistance through inhibition of IRS1. In the current study, the protein expressions of IRS1, PI3K, AKT, and JNK were detected by western blotting. The results of our study showed that the hypoglycemic activity of PQ-MGR could be mediated by increasing glucose uptake and ameliorating insulin resistance, which might be associated with the IRS1/PI3K/AKT and JNK signaling pathway.

PPAR$_\gamma$ is a member of nuclear hormone receptors, which is distributed mainly in fat, skeletal muscle, and the liver. It plays a critical role in regulating glucose and lipid metabolism.[42] GLUT4 is an insulin-regulated glucose transporter that plays an important role in the regulation of glucose homeostasis.[11] Previous studies have found that PPAR$_\gamma$ could improve glucose metabolism, reduce hyperglycemia, and ameliorate insulin resistance by enhancing the expression of GLUT4.[43,44] In our study, PQ-MGR treatment increased protein expression of GLUT4 and PPAR$_\gamma$ in the skeletal muscle and liver of diabetic mice. The results suggested that PQ-MGR increases insulin sensitivity by upregulating GLUT4 and PPAR$_\gamma$ protein expression.

AMPK is a critical regulator of glucose and fatty acid catabolism and plays an important role in diabetes through the

https://doi.org/10.1021/acsomega.1c04656
ACS Omega 2021, 6, 33652−33664

regulation of cellular energy balance and maintenance of lipid homeostasis.[45] Activation of AMPK stimulates fatty acid oxidation, reduces hepatic steatosis, and improves insulin action.[18] AMPK is activated by phosphorylation of threonine 172 (Thr172) on the α catalytic subunit.[7] Acetyl-CoA carboxylase (ACC), an important downstream effector in the AMPK signaling pathway, has played a key role in hepatic lipid synthesis, storage, and oxidation.[45] Recent studies have shown that AMPK inhibits fatty acid synthesis and improves fatty acid oxidation by phosphorylation of ACC at serine residue (Ser79).[46] In this study, PQ-MGR treatment increased the phosphorylation expression of AMPK and downstream substrate ACC. These results demonstrated that the antihypolipidemic effect of PQ-MGR might be related to the activation of the AMPK/ACC pathway.

In summary, our findings showed that treatment with PQ-MGR could remarkably reduce fasting blood glucose and serum lipid levels and ameliorate insulin resistance in HFD/STZ-induced T2DM mice. Further mechanism studies indicate that the hypoglycemic effect of PQ-MGR may be related to the IRS1/PI3K/AKT and PPAR$_\gamma$/GLUT4 signaling pathways. The activation of the AMPK/ACC signaling pathway might be associated with the hypolipidemia activity of PQ-MGR. Therefore, we suggest that PQ-MGR could be used as a potential functional food for T2DM treatment.

EXPERIMENTAL SECTION

Chemicals and Reagents. The root of *P. quinquefolius* L. samples was obtained from the Fusong County (Jilin Province, China) and identified by Professor Yi-Nan Zheng, from the College of Chinese Material Medicine, Jilin Agricultural University. Streptozotocin (STZ) was purchased from Sigma-Aldrich (St Louis, MO). All other chemicals and reagents were of analytical grade and purchased from Sinopharm (Shanghai, China). ELISA kit for fasting serum insulin (FINS) was purchased from Linco Research, Inc. (St. Charles, MO). Reagent kits for the determination of low-density lipoprotein cholesterol (LDL-C), high-density lipoprotein cholesterol (HDL-C), total cholesterol (TC), triglyceride (TG), serum alanine aminotransferase (ALT), aspartate transferase (AST), and superoxide dismutase (SOD) were obtained from Nanjing Jiancheng Bioengineering Institute (Nanjing, China). The primary anti-IRS1, anti-p-IRS1 (Ser307), anti-PI3K, anti-p-PI3K p85 (Tyr458), anti-Akt, anti-p-Akt (Ser473), anti-JNK, anti-p-JNK (Thr183/Tyr185), anti-AMPK, anti-p-AMPK (Thr172), anti-ACC, anti-p-ACC (Ser79), anti-GLUT4, anti-PPAR$_\gamma$, and anti-β-Actin antibodies were purchased from Abcam (Abcam Cambridge, U.K.).

Method of PQ-MGR Extraction. The crushed roots of American ginseng (3 kg) were extracted three times by ultrasonic-assisted extraction with 75% (v/v) methanol (MeOH)−water at room temperature (25 °C) for 45 min. The methanolic extract was concentrated in a vacuum rotary evaporator under reduced pressure at 45 °C. The distilled water was then added in concentrated methanolic extract. After defatted with petroleum ether (PE) to remove the fatty material, the water layer was further extracted with aqueous saturated *n*-BuOH to obtain *n*-BuOH and aqueous fractions, respectively. The aqueous fraction was suspended in water and loaded onto a D-101 macroporous resin column eluting with different MeOH-H_2O gradients to afford a crude PQ-MGR fraction (collecting 50% MeOH-H_2O fractions); then, the PQ-MGR fraction was further purified with cation exchange resin (SP20ss, H+ form) to obtain PQ-MGR extract (42 g). The purified PQ-MGR extract was analyzed by HPLC-UV and HPLC-MS/MS and identified by comparison of retention times with those of the authentic compounds.

HPLC Analysis. Chromatography was conducted on a Shimadzu LC 20A HPLC system (Shimadzu Corp, Japan) equipped with a binary pump and a UV detector. The liquid chromatographic separation was achieved using a Cosmosil 5 C_{18} analytical column (5 μm, 4.6 mm × 250 cm). The column temperature was kept at 30 °C, and the wavelength was detected at 203 nm. The mobile phase consisting of 50 mmol/L KH_2PO_4 (A) and acetonitrile (B) was applied with the optimized gradient elution as follows: 21.5% B at 0−21 min, 21.5−28% B at 21−26 min, 28% B at 26−44 min, 28−36% B at 44−54 min, 36−50% B at 54−60 min, 50−60% B at 60−70 min. The flow rate was set at 1.0 mL/min. The 20 μL sample solutions were directly injected into the chromatographic column manually.

HPLC/ESI-MS Analysis. HPLC-ESI-MS analyses were performed with an Agilent 1200 series HPLC system (Agilent, Waldron, Germany) coupled to an Agilent 6310 ion-trap mass spectrometer with electrospray ionization (ESI) source, operated under negative-ion mode. The conditions of the ESI source were as follows: capillary voltage, 3500 V; drying gas (N_2), 9 L/min; drying gas temperature, 350 °C; nebulizer pressure, 35 psig; source temperature, 120 °C; mass range, m/z 150−2000. The chromatography separation was also achieved using a Cosmosil 5 C_{18} analytical column. The mobile phase consisted of solvent A (0.1% formic acid in ultrapure water, v/v) and solvent B (0.1% formic acid in acetonitrile, v/v) with gradient elution (0−60 min, 15−50% B).

Animals. C57BL/6J male mice (body weight: 20 ± 2 g) were obtained from Beijing Vital River Laboratory Animal Technology Co., Ltd (Beijing, China). The animals were housed in a specific pathogen-free animal laboratory of the Experimental Animal Center of Jilin Agricultural University. The animals were kept at 22−26 °C and 50−60% relative humidity with 12 h light and dark cycles and allowed ad libitum access to feed and water. They were acclimated to the above environment for at least 7 days before the start of experimentation. The methods used in this experiment were performed in accordance with the guidelines for the care and use of animals approved by the Animal Ethics Committee of Jilin Agricultural University (No. 2019 04 09 002).

Induction of T2DM. After acclimatization, 10 mice were randomly separated as the normal control group (NC group) and given a normal chow diet (13% kcal from fat). In contrast, the other mice were fed on a high-fat diet (60% kcal from fat) with sufficient food and water for 4 weeks. The mice then fasted for 12 h and received a single intraperitoneal (ip) injection of freshly prepared streptozotocin (STZ) (Sigma-Aldrich), dissolved in cold citrate buffer (0.1 M, pH 4.5) at 100 mg/kg BW. After STZ injection, diabetic mice were maintained on an HFD for an additional 4 weeks. Mice with FBG >11.1 mmol/L were considered as diabetic mice and used in pharmacological studies.

Experimental Design. In this experiment, a total of 40 mice (10 normal; 30 STZ-induced diabetic mice) were used and were divided into four groups of 10 mice each: group I: normal control mice administered saline (NC); group II: diabetic control mice administered saline (DC); group III: diabetic mice administered PQ-MGR (300 mg/kg, body weight) (PQ-MGR300); group IV: diabetic mice administered

https://doi.org/10.1021/acsomega.1c04656
ACS Omega 2021, 6, 33652−33664

PQ-MGR (100 mg/kg, body weight) (PQ-MGR 100). The PQ-MGR group was administrated by oral gavage with PQ-MGR 100 and 300 mg/kg/day for 5 weeks. Body weight in each cage was monitored every day. At the end of the experiment, blood samples were obtained after overnight fasting (12−16 h). Then, all of the mice were sacrificed by cervical dislocation. Plasma was separated by centrifugation at 3500 rpm for 15 min at 4 °C. After centrifugation, plasma was collected and immediately stored at −80 °C. The liver, pancreas, adipose, and skeletal muscle were removed and frozen at −80 °C until analyzed or stored in formalin solution for histopathological study.

Measurement of Fasting Blood Glucose and Oral Glucose Tolerance Test. FBG levels were monitored once a week during the 5-week experimental period using a One-touch Ultra Glucometer (Johnson & Johnson) after fasting for 12 h. At the 5th week of the experiment, the mice in all groups were subjected to an oral glucose tolerance test (OGTT). Overnight-fasted mice were orally administered with glucose (2 g/kg, body weight). Blood samples were obtained from the tail vein at 0, 30, 60, and 120 min after glucose administration, and the glucose levels were evaluated using a glucometer. The area under the curve of the OGTT ($AUC_{glucose}$) was calculated using the trapezoidal rule.

Biochemical Analysis. The FINS was measured by commercial ELISA kits. The homeostatic model assessment of insulin resistance (HOMA-IR) was calculated as follows: HOMA-IR = FBG (mmol/L) × FINS (mIU/mL)/22.5. Serum levels of LDL-C, HDL-C, TC, TG, ALT, AST, and SOD were evaluated using kits according to the manufacturer's instructions.

Histopathology Analysis. The liver, pancreas, and adipose were removed from mice killed after 5 weeks of administration, immediately stored in 4% formaldehyde, then embedded in paraffin, and cut into 5 μm thick sections. The sections were stained with hematoxylin−eosin (H&E) to study the histopathological changes. In addition, the frozen sections of 8 μm thickness were stained with Oil Red O for lipid droplet analysis. Thereafter, the samples were imaged using a light microscope at 400× magnification.

Western Blot Analysis. Using the proteasome inhibitor tissue lysate RIPA, skeletal muscle and liver tissue were crushed by homogenate on the ice. The homogenization buffer was moved to a centrifuge tube, cooled on ice for 30 min, and centrifuged at 12 000 rpm for 10 min at 4 °C to get the supernatant. The protein concentrations were determined using the bicinchoninic acid (BCA) protein assay. The tissue protein (30 μg) was separated by 10% of sodium dodecyl sulfate-polyacrylamide gel electrophoresis (SDS-PAGE) and electrotransferred onto poly(vinylidene difluoride) (PVDF); the membranes were blocked with 5% skim milk for 2 h and incubated with primary antibodies (diluted 1:1000) at 4 °C overnight. After washing with TBST for 4 times, 8 min each time, the membranes were incubated with horseradish peroxidase (HRP)-conjugated secondary antibodies (diluted 1:4000) for 1.5 h at room temperature. Finally, electro-generated chemiluminescence (ECL) was used to visualize the bands.

Statistical Analysis. The data of all experiments were expressed as mean ± standard deviation (SD). Statistical analyses were performed using SPSS 18.0 (SPSS, Chicago, IL). The statistical significance of differences between experimental groups was determined by one-way analysis of variance (ANOVA). A value of $p < 0.05$ was considered significant.

AUTHOR INFORMATION

Corresponding Authors

Zhi Liu − *College of Chinese Medicinal Materials, Jilin Agricultural University, Changchun 130118, China; Institute of Agricultural Modernization, Jilin Agricultural University, Changchun 130118, China;* orcid.org/0000-0002-9690-3233; Email: lzhiiu@126.com

Guang-Zhi Sun − *Institute of Agricultural Modernization, Jilin Agricultural University, Changchun 130118, China;* Email: gzsun1967@yahoo.com

Authors

Chun-Yuan Qu − *College of Chinese Medicinal Materials, Jilin Agricultural University, Changchun 130118, China*

Jia-Xin Li − *College of Chinese Medicinal Materials, Jilin Agricultural University, Changchun 130118, China*

Yan-Fang Wang − *College of Chinese Medicinal Materials, Jilin Agricultural University, Changchun 130118, China*

Wei Li − *College of Chinese Medicinal Materials, Jilin Agricultural University, Changchun 130118, China;* orcid.org/0000-0002-2988-4298

Chong-Zhi Wang − *Tang Center for Herbal Medicine Research and The Pritzker School of Medicine, University of Chicago, Chicago, Illinois 60637, United States*

Dong-Sheng Wang − *College of Chinese Medicinal Materials, Jilin Agricultural University, Changchun 130118, China*

Jia Song − *College of Chinese Medicinal Materials, Jilin Agricultural University, Changchun 130118, China*

Chun-Su Yuan − *Tang Center for Herbal Medicine Research and The Pritzker School of Medicine, University of Chicago, Chicago, Illinois 60637, United States*

Complete contact information is available at: https://pubs.acs.org/10.1021/acsomega.1c04656

Author Contributions

‖Z.L. and C.-Y.Q. contributed equally to this work as the co-first author.

Notes

The authors declare no competing financial interest.

ACKNOWLEDGMENTS

This work was supported by grants from the National Natural Science Foundation of China (no. 31770378), Jilin Provincial Natural Science Foundation of China (no. 20180101183JC), the Jilin Science and Technology Development Plan (no. 20200301037RQ), and Tang Foundation for Research of Traditional Chinese Medicine.

ABBREVIATIONS USED

T2DM, type 2 diabetes mellitus
STZ, streptozotocin
TG, triglyceride
NEFA, nonesterified fatty acid
AST, aspartate transaminase
IRS1, insulin receptor substrate-1
Akt, protein-kinase B
AMPK, AMP-activated protein kinase
HFD, high-fat diet
FBG, fasting blood glucose

TC, total cholesterol
SOD, superoxide dismutase
ALT, alanine transaminase
PI3K, phosphoinositide3-kinase
JNK, C-Jun N-terminal kinases
ACC, acetyl-CoA carboxylase

REFERENCES

(1) Chandran, R.; Parimelazhagan, T.; Shanmugam, S.; Thankarajan, S. Antidiabetic activity of *Syzygium calophyllifolium* in Streptozotocin-Nicotinamide induced Type-2 diabetic rats. *Biomed. Pharmacother.* **2016**, *82*, 547−554.

(2) Zhao, X. M.; Wang, D. Y.; Qin, L. J.; Yang, X. Z.; Gao, C. Y. Comparative investigation for hypoglycemic effects of polysaccharides from four substitutes of *Lonicera japonica* in Chinese medicine. *Int. J. Biol. Macromol.* **2018**, *109*, 12−20.

(3) Liu, L.; Tang, D.; Zhao, H. Q.; Xin, X. L.; Aisa, H. A. Hypoglycemic effect of the polyphenols rich extract from *Rose rugosa* Thunb on high fat diet and STZ induced diabetic rats. *J. Ethnopharmacol.* **2017**, *200*, 174−181.

(4) Saeedi, P.; Petersohn, I.; Salpea, P.; Malanda, B.; Karuranga, S.; Unwin, N.; Colagiuri, S.; Guariguata, L.; Motala, A. A.; Ogurtsova, K.; Shaw, J. E.; Bright, D.; Williams, R.; IDF Diabetes Atlas Committee. Global and regional diabetes prevalence estimates for 2019 and projections for 2030 and 2045: Results from the International Diabetes Federation Diabetes Atlas, 9(th) edition. *Diabetes Res. Clin. Pract.* **2019**, *157*, No. 107843.

(5) Lu, A. X.; Yu, M. G.; Fang, Z. Y.; Xiao, B.; Guo, L.; Wang, W. M.; Li, J.; Wang, S.; Zhang, Y. J. Preparation of the controlled acid hydrolysates from pumpkin polysaccharides and their antioxidant and antidiabetic evaluation. *Int. J. Biol. Macromol.* **2019**, *121*, 261−269.

(6) Cui, L. J.; Liu, M.; Chang, X. Y.; Sun, K. The inhibiting effect of the *Coptis chinensis* polysaccharide on the type II diabetic mice. *Biomed. Pharmacother.* **2016**, *81*, 111−119.

(7) Xu, J.; Wang, S.; Feng, T. H.; Chen, Y.; Yang, G. Z. Hypoglycemic and hypolipidemic effects of total saponins from *Stauntonia chinensis* in diabetic db/db mice. *J. Cell. Mol. Med.* **2018**, *22*, 6026−6038.

(8) Ma, C. Y.; Yu, H. Y.; Xiao, Y.; Wang, H. J. *Momordica charantia* extracts ameliorate insulin resistance by regulating the expression of SOCS-3 and JNK in type 2 diabetes mellitus rats. *Pharm. Biol.* **2017**, *55*, 2170−2177.

(9) Li, S. Q.; Chen, H. X.; Wang, J.; Wang, X. M.; Hu, B.; Lv, F. N. Involvement of the PI3K/Akt signal pathway in the hypoglycemic effects of tea polysaccharides on diabetic mice. *Int. J. Biol. Macromol.* **2015**, *81*, 967−974.

(10) Fan, Y. B.; He, Z. W.; Wang, W.; Li, J. J.; Hu, A. M.; Li, L.; Yan, L.; Li, Z. J.; Yin, Q. Tangganjian decoction ameliorates type 2 diabetes mellitus and nonalcoholic fatty liver disease in rats by activating the IRS/PI3K/AKT signaling pathway. *Biomed. Pharmacother.* **2018**, *106*, 733−737.

(11) Sun, H. L.; Liu, X. X.; Long, S. R.; Teng, W.; Ge, H. N.; Wang, Y.; Yu, S. C.; Xue, Y.; Zhang, Y. J.; Li, X.; Li, W. J. Antidiabetic effects of pterostilbene through PI3K/Akt signal pathway in high fat diet and STZ-induced diabetic rats. *Eur. J. Pharmacol.* **2019**, *859*, No. 172526.

(12) Yuan, Q. C.; Zhan, B. Y.; Du, M.; Chang, R.; Li, T. G.; Mao, X. Y. Dietary milk fat globule membrane regulates JNK and PI3K/Akt pathway and ameliorates type 2 diabetes in mice induced by a high-fat diet and streptozotocin. *J. Funct. Foods* **2019**, *60*, No. 103435.

(13) Solinas, G.; Becattini, B. JNK at the crossroad of obesity, insulin resistance, and cell stress response. *Mol. Metab.* **2017**, *6*, 174−184.

(14) Tanti, J. F.; Grémeaux, T.; van Obberghen, E.; Le Marchand-Brustel, Y. Serine/threonine phosphorylation of insulin receptor substrate 1 modulates insulin receptor signaling. *J. Biol. Chem.* **1994**, *269*, 6051−6057.

(15) Liu, Y.; Deng, J. J.; Fan, D. D. Ginsenoside Rk_3 ameliorates high-fat-diet/streptozocin induced type 2 diabetes mellitus in mice via the AMPK/Akt signaling pathway. *Food Funct.* **2019**, *10*, 2538−2551.

(16) Nie, X. Q.; Chen, H. H.; Zhang, J. Y.; Zhang, Y. J.; Yang, J. W.; Pan, H. J.; Song, W. X.; Murad, F.; He, Y. Q.; Bian, K. Rutaecarpine ameliorates hyperlipidemia and hyperglycemia in fat-fed, streptozotocin-treated rats via regulating the IRS-1/PI3K/Akt and AMPK/ACC2 signaling pathways. *Acta Pharmacol. Sin.* **2016**, *37*, 483−496.

(17) Shi, T.; Fan, G. Q.; Xiao, S. D. SIRT3 reduces lipid accumulation via AMPK activation in human hepatic cells. *J. Dig. Dis.* **2010**, *11*, 55−62.

(18) Xiong, H.; Zhang, S. N.; Zhao, Z. Q.; Zhao, P.; Chen, L. Y.; Mei, Z. N. Antidiabetic activities of entagenic acid in type 2 diabetic db/db mice and L6 myotubes via AMPK/GLUT4 pathway. *J. Ethnopharmacol.* **2018**, *211*, 366−374.

(19) Huang, X.; Liu, Y.; Zhang, Y.; Li, S. P.; Yue, H.; Chen, C. B.; Liu, S. Y. Multicomponent assessment and ginsenoside conversions of *Panax quinquefolium* L. roots before and after steaming by HPLC-MS^n. *J. Ginseng Res.* **2019**, *43*, 27−37.

(20) Attele, A. S.; Wu, J. A.; Yuan, C. S. Ginseng pharmacology: Multiple constituents and multiple actions. *Biochem. Pharmacol.* **1999**, *58*, 1685−1693.

(21) Yuan, C. S.; Wang, C. Z.; Wicks, S. M.; Qi, L. W. Chemical and pharmacological studies of saponins with a focus on American ginseng. *J. Ginseng Res.* **2010**, *34*, 160−167.

(22) Shao, Z. H.; Xie, J. T.; Vanden Hoek, T. L.; Mehendale, S.; Aung, H.; Li, C. Q.; Qin, Y. M.; Schumacker, P. T.; Becker, L. B.; Yuan, C. S. Antioxidant effects of American ginseng berry extract in cardiomyocytes exposed to acute oxidant stress. *Biochim. Biophys. Acta, Gen. Subj.* **2004**, *1670*, 165−171.

(23) Qi, L. W.; Wang, C. Z.; Yuan, C. S. Ginsenosides from American ginseng: chemical and pharmacological diversity. *Phytochemistry* **2011**, *72*, 689−699.

(24) Liu, Z.; Xia, J.; Wang, C. Z.; Zhang, J. Q.; Ruan, C. C.; Sun, G. Z.; Yuan, C. S. Remarkable Impact of Acidic Ginsenosides and Organic Acids on Ginsenoside Transformation from Fresh Ginseng to Red Ginseng. *J. Agric. Food Chem.* **2016**, *64*, 5389−5399.

(25) Yang, C. S.; Li, C. J.; Wei, W.; Wei, Y. J.; Liu, Q. F.; Zhao, G. P.; Yue, J. M.; Yan, X.; Wang, P. P.; Zhou, Z. H. The unprecedented diversity of UGT94-family UDP-glycosyltransferases in Panax plants and their contribution to ginsenoside biosynthesis. *Sci. Rep.* **2020**, *10*, No. 15394.

(26) Guo, R.; Wang, L.; Zeng, X. Q.; Liu, M. H.; Zhou, P.; Lu, H. X.; Lin, H. L.; Dong, M. Aquaporin 7 involved in GINSENOSIDE-RB1-mediated anti-obesity via peroxisome proliferator-activated receptor gamma pathway. *Nutr. Metab.* **2020**, *17*, No. 69.

(27) Zhou, P.; Xie, W. J.; He, S. B.; Sun, Y. F.; Meng, X. B.; Sun, G. B.; Sun, X. B. Ginsenoside Rb1 as an Anti-Diabetic Agent and Its Underlying Mechanism Analysis. *Cells* **2019**, *8*, No. 204.

(28) Dai, S. S.; Hong, Y. L.; Xu, J.; Lin, Y.; Si, Q. Y.; Gu, X. J. Ginsenoside Rb2 promotes glucose metabolism and attenuates fat accumulation via AKT-dependent mechanisms. *Biomed. Pharmacother.* **2018**, *100*, 93−100.

(29) Lee, K. T.; Jung, T. W.; Lee, H. J.; Kim, S. G.; Shin, Y. S.; Whang, W. K. The antidiabetic effect of ginsenoside Rb_2 via activation of AMPK. *Arch. Pharm. Res.* **2011**, *34*, 1201−1208.

(30) Xie, J. T.; Mehendale, S. R.; Li, X. M.; Quigg, R.; Wang, X. Y.; Wang, C. Z.; Wu, J. A.; Aung, H. H.; Rue, P. A.; Bell, G. I.; Yuan, C. S. Anti-diabetic effect of ginsenoside Re in ob/ob mice. *Biochim. Biophys. Acta, Mol. Basis Dis.* **2005**, *1740*, 319−325.

(31) Kim, J. M.; Park, C. H.; Park, S. K.; Seung, T. W.; Kang, J. Y.; Ha, J. S.; Lee, D. S.; Lee, U.; Kim, D. O.; Heo, H. J. Ginsenoside Re Ameliorates Brain Insulin Resistance and Cognitive Dysfunction in High Fat Diet-Induced C57BL/6 Mice. *J. Agric. Food Chem.* **2017**, *65*, 2719−2729.

(32) Li, J. X.; Li, M. Y.; L, Z. D.; Wen, X.; Qu, C. Y.; Liu, Z. Determination of malonyl ginsenoside in *Panax quinquefolius* L. with different growth ages and parts by HPLC. *Chin. Tradit. Pat. Med.* **2020**, *40*, 2675−3679.

(33) Fuzzati, N. Analysis methods of ginsenosides. *J. Chromatogr. B* **2004**, *812*, 119−133.

https://doi.org/10.1021/acsomega.1c04656
ACS Omega 2021, 6, 33652−33664

(34) Paramasivan, S.; Adav, S. S.; Ngan, S. C.; Dalan, R.; Leow, M. K. S.; Ho, H. H.; Sze, S. K. Serum albumin cysteine trioxidation is a potential oxidative stress biomarker of type 2 diabetes mellitus. *Sci. Rep.* **2020**, *10*, No. 6475.
(35) Hwang, Y. C.; Oh, D. H.; Choi, M. C.; Lee, S. Y.; Ahn, K. J.; Chung, H. Y.; Lim, S. J.; Chung, S. H.; Jeong, I. K. Compound K attenuates glucose intolerance and hepatic steatosis through AMPK-dependent pathways in type 2 diabetic OLETF rats. *Korean J. Intern. Med.* **2018**, *33*, 347−355.
(36) Oza, M. J.; Kulkarni, Y. A. Biochanin A improves insulin sensitivity and controls hyperglycemia in type 2 diabetes. *Biomed. Pharmacother.* **2018**, *107*, 1119−1127.
(37) Mooradian, A. D. Dyslipidemia in type 2 diabetes mellitus. *Nat. Rev. Endocrinol.* **2009**, *5*, 150−159.
(38) de Moura Barbosa, H.; Amaral, D.; do Nascimento, J. N.; Machado, D. C.; de Sousa Araujo, T. A.; de Albuquerque, U. P.; Guedes da Silva Almeida, J. R.; Rolim, L. A.; Lopes, N. P.; Gomes, D. A.; Lira, E. C. *Spondias tuberosa* inner bark extract exert antidiabetic effects in streptozotocin-induced diabetic rats. *J. Ethnopharmacol.* **2018**, *227*, 248−257.
(39) Kim, D. H.; Kim, S. J.; Yu, K. Y.; Jeong, S. I.; Kim, S. Y. Anti-hyperglycemic effects and signaling mechanism of *Perilla frutescens* sprout extract. *Nutr. Res. Pract.* **2018**, *12*, 20−28.
(40) Yang, C. F.; Lai, S. S.; Chen, Y. H.; Liu, D.; Liu, B.; Ai, C.; Wan, X. Z.; Gao, L. Y.; Chen, X. H.; Zhao, C. Anti-diabetic effect of oligosaccharides from seaweed *Sargassum confusum* via JNK-IRS1/PI3K signalling pathways and regulation of gut microbiota. *Food Chem. Toxicol.* **2019**, *131*, No. 110562.
(41) Chen, Y. Q.; Liu, D.; Wang, D. Y.; Lai, S. S.; Zhong, R. T.; Liu, Y. Y.; Yang, C. F.; Liu, B.; Sarker, M. R.; Zhao, C. Hypoglycemic activity and gut microbiota regulation of a novel polysaccharide from *Grifola frondosa* in type 2 diabetic mice. *Food Chem. Toxicol.* **2019**, *126*, 295−302.
(42) Guo, Y.; Dai, R. J.; Deng, Y. L.; Sun, L. L.; Meng, S. Y.; Xin, N. Hypoglycemic activity of the extracts of *Belamcanda chinensis* leaves (BCLE) on KK- A^y mice. *Biomed. Pharmacother.* **2019**, *110*, 449−455.
(43) Singh, A. K.; Raj, V.; Keshari, A. K.; Rai, A.; Kumar, P.; Rawat, A.; Maity, B.; Kumar, D.; Prakash, A.; De, A.; Samanta, A.; Bhattacharya, B.; Saha, S. Isolated mangiferin and naringenin exert antidiabetic effect via PPARgamma/GLUT4 dual agonistic action with strong metabolic regulation. *Chem.-Biol. Interact.* **2018**, *280*, 33−44.
(44) Kim, J. C. The effect of exercise training combined with PPARγ agonist on skeletal muscle glucose uptake and insulin sensitivity in induced diabetic obese Zucker rats. *J. Exercise Nutr. Biochem.* **2016**, *20*, 42−50.
(45) Gao, D.; Zhang, Y. L.; Yang, F. Q.; Li, F.; Zhang, Q. H.; Xia, Z. N. The flower of *Edgeworthia gardneri* (wall.) Meisn. suppresses adipogenesis through modulation of the AMPK pathway in 3T3-L1 adipocytes. *J. Ethnopharmacol.* **2016**, *191*, 379−386.
(46) Galic, S.; Loh, K.; Murray-Segal, L.; Steinberg, G. R.; Andrews, Z. B.; Kemp, B. E. AMPK signaling to acetyl-CoA carboxylase is required for fasting- and cold-induced appetite but not thermogenesis. *eLife* **2018**, *7*, No. e32656.

https://doi.org/10.1021/acsomega.1c04656
ACS Omega 2021, 6, 33652−33664